THE JOURNAL OF BIOLOGICAL CHEMISTRY VOL. 289, NO. 32, pp. 22524–22535, August 8, 2014

Motor-mediated Cortical *versus* Astral Microtubule Organization in Lipid-monolayered Droplets[S]

Received for publication, May 16, 2014, and in revised form, June 20, 2014 Published, JBC Papers in Press, June 25, 2014, DOI 10.1074/jbc.M114.582015

Hella Baumann[1] **and Thomas Surrey**[2]

From the London Research Institute, Cancer Research UK, 44 Lincoln's Inn Fields, London WC2A 3LY, United Kingdom

Background: How cytoskeleton architecture is established within the confining boundary of the cell membrane is not understood.
Results: Together, spatial constraints and cross-linking motor activities determine distinct motor/microtubule organizations in a biomimetic system.
Conclusion: Characteristic microtubule architectures result from basic design principles.
Significance: Spatial confinement plays an important role in cytoskeleton organization.

The correct spatial organization of microtubules is of crucial importance for determining the internal architecture of eukaryotic cells. Microtubules are arranged in space by a multitude of biochemical activities and by spatial constraints imposed by the cell boundary. The principles underlying the establishment of distinct intracellular architectures are only poorly understood. Here, we studied the effect of spatial confinement on the self-organization of purified motors and microtubules that are encapsulated in lipid-monolayered droplets in oil, varying in diameter from 5–100 μm, which covers the size range of typical cell bodies. We found that droplet size alone had a major organizing influence. The presence of a microtubule-crosslinking motor protein decreased the number of accessible types of microtubule organizations. Depending on the degree of spatial confinement, the presence of the motor caused either the formation of a cortical array of bent microtubule bundles or the generation of single microtubule asters in the droplets. These are two of the most prominent forms of microtubule arrangements in plant and metazoan cells. Our results provide insights into the combined organizing influence of spatial constraints and cross-linking motor activities determining distinct microtubule architectures in a minimal biomimetic system. In the future, this simple lipid-monolayered droplet system characterized here can be expanded readily to include further biochemical activities or used as the starting point for the investigation of motor-mediated microtubule organization inside liposomes surrounded by a deformable lipid bilayer.

The correct architecture of the microtubule cytoskeleton in living cells is essential for correct organelle positioning, cell division, and cell differentiation. The spatial organization of microtubules is determined by biochemical activities, for example from nucleators, microtubule dynamics regulators, cross-linkers and molecular motors, but also by the presence of the cell boundary (1–3). The principles underlying the establishment of distinct intracellular architectures are only poorly understood. This is largely due to the complexity of the repertoire of activities involved and due to an underrepresentation of studies directly addressing the effects of spatial confinement.

In vitro reconstitution approaches are useful for the investigation of the design principles of simpler model systems of known composition that consist of small sets of well characterized purified components. Previously, *in vitro* experiments with purified microtubule cross-linking and sliding motors showed under which conditions motors organize microtubules into bundles, asters, or networks of focused poles in quasi-two-dimensional unconfined environments (4–7). The interplay between a confining boundary and growing microtubules was first studied *in vitro* for individual microtubules that were encapsulated in small liposomes produced by a freeze-thaw method (8, 9) and, later, in microfabricated chambers (10). Depending on geometrical constraints, straight microtubules either deformed the membrane or the microtubules were bent by the curved membrane (8, 9) or the hard boundary of the microchamber (10). The positioning of asters consisting of multiple microtubules that were grown from microtubule-organizing centers was investigated in microchambers (11, 12). Geometrical constraints imposed by microtubule length and the size of the undeformable chamber as well as the dynamic properties of the microtubules determined the positioning of the asters in the microchamber (11, 12).

Micrometer-sized droplets in oil are an alternative system to encapsulate biochemical reactions (13) and to study the effects of confinement. Such droplets can be produced easily, and they can have lipid-monolayered boundaries that mimic the inner surface of the plasma membrane. Lipid-monolayered droplets can then be transformed into liposomes (14). This method has been used recently for the reconstitution of an active actin cortex inside liposomes consisting of a defined set of purified proteins of the actin cytoskeleton (15, 16). Comparable experiments for encapsulated active motor/microtubule assemblies produced with purified proteins are lacking. The droplets-in-oil method has been used to investigate self-organized microtubule assemblies in encapsulated *Xenopus* egg extract, an experimental system of a highly complex composition (17). When the microtubule stabilizer paclitaxel is added to such

[S] This article contains supplemental Movies 1–10.
[1] Supported by the Boehringer-Ingelheim Fonds.
[2] Supported by Cancer Research UK and the European Research Council. To whom correspondence should be addressed. E-mail: thomas.surrey@cancer.org.uk.

Xenopus egg extracts in the absence of confinement, microtubule asters are generated by a set of microtubule cross-linking and sliding activities, including the motor protein dynein (18, 19). Aster formation in encapsulated extract has been shown to depend on confinement size. Spatial constraints led to microtubule bundling and bending in small droplets (17). A systematic investigation, however, of how microtubules arrange in droplets of different sizes in the absence of any other proteins, and how the presence of a purified and well characterized microtubule sliding motor changes these arrangements, is currently lacking.

Here we have studied the effect of confinement on the self-organization of purified motors and microtubules that are encapsulated in lipid-monolayered droplets in oil. We observed that a relatively large variety of microtubule arrangements is accessible in the absence of a microtubule cross-linking motor and that, in this case, droplet size had the major organizing effect. The bundling and sliding activity of a motor protein restricted access to several arrangements and, additionally, opened the motor-dependent pathway for aster organization, provided the droplets were of sufficient size. These results provide insight into the combined ordering effects of spatial constraints and cross-linking motor activities on microtubule organization in a minimal biomimetic system.

EXPERIMENTAL PROCEDURES

Protein Biochemistry—Pig brain tubulin was purified and labeled with Atto633-*N*-hydroxy succinimidylester (Sigma) using standard methods (20, 21). In all experiments, the final labeling ratio of the tubulin mixture was adjusted to 0.1 fluorophores/tubulin dimer. Concentrations and labeling ratios were measured by absorbance at 280 and 629 nm using the appropriate extinction coefficients. Tubulin concentrations are tubulin dimer concentrations throughout.

mCherry-tagged *Xenopus laevis* kinesin-14 XCTK2 (mCherry-kinesin-14) was produced essentially as described previously (4, 22) with the following modifications. Insect cells with baculovirus-overexpressed His_6-mCherry-kinesin-14 were homogenized manually in buffer A (50 mM $NaPO_4$ buffer, 300 mM KCl, 1 mM $MgCl_2$, 1 mM EGTA, and 2.5 mM 2-mercaptoethanol (pH 7)) supplemented with 30 mM imidazole, 0.5 mM ATP, and complete EDTA-free protease inhibitors (Roche). The protein was eluted from Protino nickel-tris(carboxymethyl)ethylene diamine) beads (Macherey-Nagel) using buffer A supplemented with 300 mM imidazole and 0.05 mM ATP. The buffer was then exchanged to buffer A supplemented with 0.05 mM ATP using a PD 10 desalting column (Fisher Scientific). The His tag was cleaved off by AcTEV protease (LifeTechnologies) overnight at 4 °C, producing mCherry-kinesin-14. The free His tag was removed using Protino nickel-tris(carboxymethyl)ethylene diamine beads, followed by gel filtration of the protein in buffer A supplemented with 0.05 mM ATP. The protein was concentrated using membrane ultracentrifugation (VivaSpin, molecular mass 30,000 Da), and aliquots were shock-frozen and stored in liquid nitrogen. The kinesin concentration was determined by Bradford (Bio-Rad) using a BSA standard. The successful cleavage of the His tag was verified by an anti-histidine Western blot analysis.

Generation of Lipid-monolayered Droplets in Oil—To generate lipid-monolayered droplets, we emulsified a solution containing proteins in a lipid/oil mixture (similar as in Refs. 14, 15). For the lipid/oil mixture, a total of 10 mg of purified lipids dissolved in chloroform (Avanti Polar Lipids) were mixed in a 25-ml round bottom glass. The following lipid mixtures were tested (Fig. 1): 100% 1,2-dioleoyl-*sn*-glycero-3-phosphocholine (DOPC);[3] 90% DOPC and 10% 1,2-dioleoyl-*sn*-glycero-3-phosphoglycerol (DOPG); 65% DOPC and 35% 1,2-dioleoyl-*sn*-glycero-3-phosphoethanolamine (DOPE); and 55% DOPC, 35% DOPE, and 10% DOPG (all are mole percent).

The chloroform was allowed to evaporate under nitrogen flow, and the lipid mixture (see below) was redissolved in 200 μl of cyclohexane, frozen in liquid nitrogen, and lyophilized at −80 °C in a freeze dryer (Labconco) for at least 12 h to remove all solvent. The dried lipids were then dissolved in 10 ml of mineral oil at a total concentration of 1 mg/ml by sonicating in an ice-cold water bath for 30 min. Exposure to air was minimized by filling the flasks with nitrogen gas. The lipid/oil mixture was left to cool at room temperature for another 30 min and stored at 4 °C for a maximum of 2 days.

To generate the final emulsion, 20 μl of a protein-containing solution (see below) was clarified by centrifugation for 3 min at 13,000 × *g* at 4 °C. 1.3 μl of clarified solution was added into 450 μl of lipid/oil mixture (prechilled to 4 °C) and sheared gently by pumping with a Microlance needle (Scientific Laboratory Supplies) fitted to a 1-ml glass syringe (Roth).

For initial optimization experiments (Fig. 1), the protein-containing solution consisted of 40 μM Atto633-labeled tubulin in droplet buffer (44 mM PIPES, 10.3 mM $MgCl_2$, 2.8 mM EGTA, 3 mM GTP, 5 mM ATP, 40 mM 2-mercaptoethanol, 50 mM KCl, 1 μM paclitaxel, 20 mM glucose, 1 mg/ml glucose oxidase (Serva, catalog no. 22778), 0.5 mg/ml catalase (Sigma, catalog no. C40), 0.5 mg/ml BSA, and 0.25 mg/ml β-casein (pH 6.8)) without or with 10% (v/v) glycerol.

For all remaining experiments (Figs. 2–7), the lipid mixture was always 55% DOPC, 35% DOPE, and 10% DOPG, and the protein-containing solution typically consisted of 40 μM labeled Atto-633 tubulin in standard droplet buffer (droplet buffer supplemented with 10% (v/v) glycerol, and 10% (v/v) XCTK2 gel filtration buffer) (Figs. 2–4). In some experiments, the tubulin concentration was changed to 30 and 50 μM (Fig. 4, *C* and *D*), and in self-organization experiments, 200 (Figs. 5–7) or 400 nM mCherry-kinesin-14 was added to the protein-containing solution.

Imaging of Microtubule Polymerization and Self-organization in Droplets—Coverslips were sonicated in 50% (v/v) ethanol, rinsed with MilliQ-water, blow-dried with nitrogen gas, immersed in Rain-X® (Shell Car Care International Ltd.), and dried in air before being fitted with PDMS matrices.

The matrices were prepared from PDMS (Sylgard 184, Dow Corning) gels using a 10:1 ratio (v/v) of elastomer:curing agent.

[3] The abbreviations used are: DOPC, 1,2-dioleoyl-*sn*-glycero-3-phosphocholine; DOPG, 1,2-dioleoyl-*sn*-glycero-3-phosphoglycerol; DOPE, 1,2-dioleoyl-*sn*-glycero-3-phosphoethanolamine; PC, phosphatidylcholine; PG, phosphatidylglycerol; PE, phosphatidylethanolamine; PDMS, polydimethylsiloxane.

Both components were mixed extensively for 1 min in a 50-ml Falcon tube, centrifuged at 4000 × *g* at 4 °C for 1 min to remove air bubbles, and then poured into a Petri dish (Falcon BD). The polymer was subsequently cured for 1 h in an oven at 75 °C, followed by 10 h at room temperature. Using a punch, round holes of 5 mm in diameter were stamped into the 3-mm-high gel. With a scalpel, 10 × 15 mm squares were cut out of the PDMS, each containing two holes separated by not more than 1.5 mm. A PDMS matrix was positioned in the middle, perpendicular to the long edge of a cleaned and Rain-X®-treated coverslip, and pressed gently onto it, allowing no gap between the glass and the PDMS gel. The PDMS chambers were placed on an ice-cold metal block, and 20 μl of the emulsion was added immediately into the wells after mixing. Droplets in oil were left to settle at 4 °C for 4 min before the sample was put under the microscope.

Images were acquired with a spinning disk confocal microscope (3I, Intelligent Imaging Innovations) comprising a LaserStack™ (containing 488 nm, 50 milliwatt; 561 nm, 50 milliwatt; and 640 nm, 40 milliwatt) Yokogawa CSU M1 on a Zeiss Axio Observer Z1 with a ×63 1.4 numerical aperture oil immersion objective (Zeiss) and a charge-coupled device camera (Orca-Flash4.0 LT). The microscope was equipped with an environmental chamber (OKOlab) that was heated to 32 °C. Time-lapse imaging was started immediately after placing the slide into the heated environment box. To minimize alterations of the measured fluorescence intensities because of a lensing effect caused by the diffractive index mismatch of the droplet buffer and the oil, the droplets were imaged close to their equatorial planes. For microtubule polymerization assays, images at four to six different positions were recorded every 60 s with 300-ms exposure times (640 nm excitation, 30% laser intensity) for 20 min. For self-organization assays, images were recorded for 25 min using multipoint acquisition every 60 s with 300-ms exposure times for Atto633 (640 nm excitation, 30% laser intensity) and 400-ms exposure times for mCherry (561 nm excitation, 50% laser intensity). End state images of one focal plane per position or three-dimensional image stacks were taken immediately after the time course. Stacks were acquired in z steps of 500 nm (exposures as above for Atto633 and mCherry). All images were acquired using 2 × 2 pixel binning.

Unconfined Microtubule Polymerization and Self-organization—For control purposes, microtubule polymerization and self-organization assays in bulk were performed in 10-μl flow chambers assembled from a poly-L-lysine-PEG-treated (SuSoS) coverslip and a glass slide using double-sided sticky tape (23). The chamber was placed on an ice-cold metal block and filled with 5% (w/v) Pluronic F-127 (Sigma). After 3 min, 30 μl of flow chamber buffer (40 mM PIPES, 0.5 mM EGTA, 0.5 mM $MgCl_2$, and 1 mg/ml BSA (pH 6.8)) followed by 20 μl of clarified assay solution were flowed through the chamber. Clarification was achieved by centrifugation for 3 min at 13,000 × g and 4 °C in a tabletop centrifuge. For microtubule polymerization assays (supplemental Movie 1), the final assay solution contained 20 μM Atto633-labeled tubulin in droplet buffer. For motor/microtubule self-organization assays (supplemental Movie 8), the final assay solution contained 7 μM Atto633-labeled tubulin and 100 nM mCherry-kinesin-14 in standard droplet buffer. The chamber was sealed with a 1:1:1 (w/w) mixture of VALAP (Vaseline, lanolin, and paraffin wax, Sigma) and used immediately used for imaging.

Imaging was done as described for droplets in oil, with the following modifications. A 40 × 1.3 numerical aperture oil immersion objective (Zeiss) was used without multipoint acquisition. For microtubule polymerization assays (supplemental Movie 1), images were recorded every 20 s with an exposure time of 100 ms (640 nm excitation) for 20 min. For self-organization assays (supplemental Movie 8), images were recorded every 20 s with 300-ms exposure times (561- and 644-nm excitation) for 20 min. Binning and laser intensities were as described above.

Image Processing—All confocal microscopy images were acquired using Slidebook software (3I, Intelligent Imaging Innovations). For optimal visualization, they were processed (signal levels and contrast adjustment before conversion from 16- to 8-bit using ImageJ (Research Service Branch, National Institutes of Health, http://rsb.info.nih.gov/ij). Three-dimensional projections and XZ plane pictures of droplets in oil were rendered from stacks in Imaris (Bitplane AG).

For movies, time-lapse confocal microscopy images were corrected for bleaching by adjusting the mean intensity of each frame using the correct_bleach ImageJ macro. Time stamps and scale bars were added after processing using the ImageJ plugins.

Frequencies of Microtubule Arrangements in Droplets of Different Sizes—To identify the end state of microtubule polymerization and motor/microtubule self-organization (the time point of the reaction after which the microtubule arrangement did not change significantly), time-lapse confocal microscopy images, taken every minute, were analyzed manually from at least 10 time courses/condition.

Microtubule arrangements inside droplets were analyzed and classified by eye on the basis of confocal slice stacks. For each condition, at least 70 stacks from 20 independent experiments over five different days (minimum) were considered. The diameter was measured using the distance between highest Atto633 dye intensities at the droplet rim from one pixel line plot in a lateral direction over the equatorial planes of the droplets. All droplets in a field of view with a diameter ≥ 2.5 μm were considered and assigned to one of the bins, each comprising a 5-μm diameter range around the indicated central value. For each droplet size category, a minimum of 10 droplets was analyzed.

RESULTS

To investigate the self-organization of microtubules and purified motors in confined environments, we produced droplets of protein-containing solutions dispersed in mineral oil (see "Experimental Procedures") (14, 15, 17). In an attempt to mimic the inner leaflet of the plasma membrane, lipids were added to the oil so that a lipid monolayer formed at the oil/droplet interface (14, 15, 17). Typical droplet sizes were in the range of ~5–100 μm in diameter, which covered the range of the typical size of cell bodies of somatic metazoan cells (13). Fluorescently labeled proteins were imaged using spinning disk confocal microscopy.

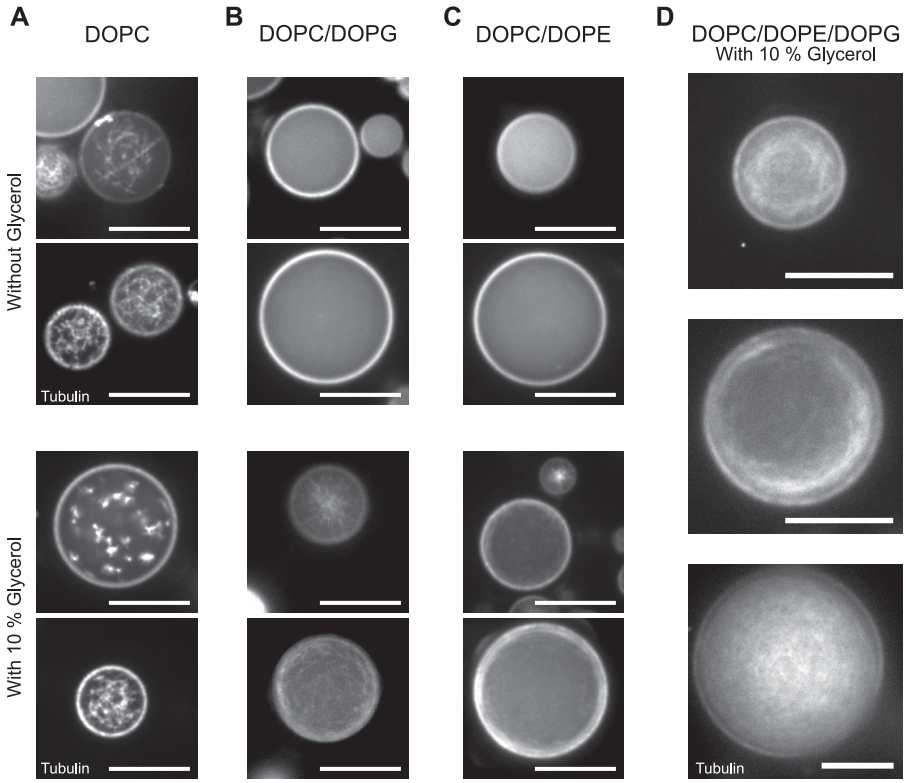

FIGURE 1. **Effect of lipid composition on microtubule polymerization.** Lipid-monolayered droplets (in mineral oil) containing 40 μM Atto633-labeled tubulin, and 3 mM GTP in droplet buffer (see "Experimental Procedures") with or without glycerol. Images of the equatorial plane of the droplets were recorded by spinning disk confocal microscopy 20 min after polymerization was triggered by a temperature shift to 32 °C. *A*, in DOPC-monolayered droplets, tubulin forms aggregates both in the absence (*top panel*) and presence of 10% glycerol (*bottom panel*). *B* and *C*, in DOPC/DOPG-monolayered droplets (*B*) and in DOPC/DOPE-monolayered droplets (*C*), tubulin neither aggregates nor polymerizes (*top panels*). However it polymerizes to microtubules in the presence of 10% glycerol (*bottom panels*). *D*, in DOPC/DOPE/DOPG-monolayered droplets, microtubules polymerize in the presence of 10% glycerol. *Scale bars* = 20 μm.

First, we investigated the conditions under which microtubules nucleated in encapsulated solutions of purified tubulin and GTP in response to a temperature shift from 4 °C to 32 °C. A low concentration of paclitaxel was added to the droplet buffer in all experiments to promote nucleation. Starting with the naturally highly abundant phospholipid DOPC (24), we found that microtubule nucleation in DOPC-monolayered droplets was less efficient in comparison with quasi-unconfined conditions. Although microtubules readily nucleated within about 1–2 min in a solution with 20 μM Atto633-labeled tubulin in a flow chamber of typical dimensions of 16 × 4 × 0.15 mm (10 μl) (supplemental Movie 1), elevated concentrations of 40 μM Atto633-labeled tubulin were required to achieve visible nucleation within comparable times in DOPC-monolayered droplets (data not shown). However, in most DOPC-monolayered droplets, tubulin also formed aggregates or short stubs that decorated longer polymerized microtubules or microtubule bundles, leading to a "stubby" appearance 20 min after the temperature shift (Fig. 1*A*, *top panel*). Glycerol, a well known microtubule-stabilizing agent (25), did not prevent this aggregation (Fig. 1*A*, *bottom panel*). Previously, actin filaments were grown from actin that was encapsulated in egg PC liposomes and where cholesterol was added to the membrane (15). However, when we added up to 35 mol% cholesterol to the mineral oil, in addition to DOPC, we still observed tubulin aggregation in lipid-monolayered droplets (data not shown).

In an attempt to suppress a potential interaction of tubulin with lipid headgroups that might trigger tubulin aggregation (26), we added 10 mol% of the negatively charged lipid DOPG to DOPC. 40 μM Atto633-tubulin inside DOPC/DOPG-monolayered droplets was now soluble, but the nucleation of microtubules was inhibited (Fig. 1*B*, *top panel*). Addition of 10% (v/v) glycerol to the buffer that was encapsulated in DOPC/DOPG-monolayered droplets efficiently stimulated microtubule nucleation within 1–2 min without inducing aggregation, even after 20 min (Fig. 1*B*, *bottom panel*). Similarly, no microtubule aggregation was observed when 35 mol% DOPE, a zwitterionic lipid that is a prominent component of metazoan plasma membranes (27), was added to the DOPC (Fig. 1*C*, *top panel*). The addition of 10% glycerol was also necessary to allow efficient microtubule nucleation from 40 μM Atto633-tubulin in these droplets (Fig. 1*C*, *bottom panel*).

The combination of DOPC, DOPE, and DOPG (55, 35, and 10 mol%, respectively), which is somewhat similar to the composition of natural plasma membranes, also resulted in the suppression of tubulin aggregation in the droplets and allowed for controlled and robust microtubule nucleation when glycerol was added to the buffer (Fig. 1*D*). We continued our studies with this lipid composition and with glycerol included in the buffer. Microtubule growth appeared to reach an end state after ~20 min (supplemental Movie 2). Interestingly, different end states could be observed that appeared to depend on droplet size. For example, although larger droplets appeared to be filled evenly with an unordered array of microtubules (Fig. 1*D*, *bottom panel*), smaller droplets often developed a cortical array of bent microtubules positioned close to the droplet boundary

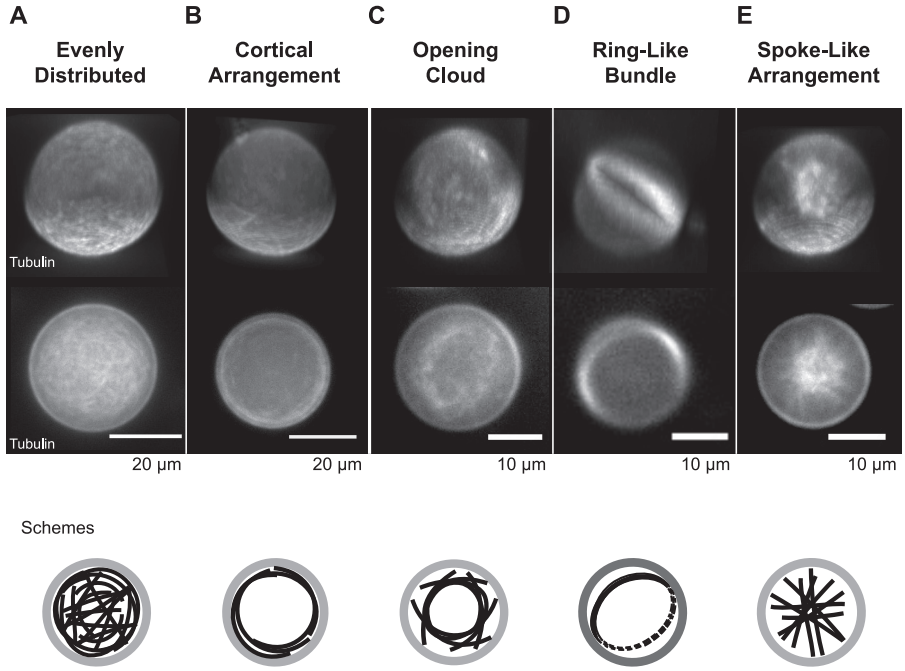

FIGURE 2. **Categories of confined microtubule arrangements.** Categorization of different microtubule arrangements inside lipid-monolayered droplets. Three-dimensional projections (*top panel*, *top row*) and images of the equatorial plane (*top panel*, *bottom row*) of Atto633-microtubules inside DOPC/DOPE/DOPG-monolayered droplets as imaged with spinning disk confocal microscopy 20 min after the polymerization reaction was started. The arrangements at end state were classified into a network of evenly distributed microtubules (*A*), a cortical arrangement (*B*), an opening cloud (*C*), a ring-like bundle (*D*), or a spoke-like arrangement (*E*). Schemes (*bottom panel*) show an interpretation for each arrangement type of microtubules (*black*) inside the lipid-monolayered droplets (*gray*). The tubulin concentration was 40 μM.

(Fig. 1*D*, *top* and *center panel*). Similar observations have been made previously for microtubules growing from pure tubulin in microfabricated chambers (10) and for microtubule bundles growing in *Xenopus* egg extract-filled droplets (17). Microtubule bending is expected for microtubules that can grow longer than the diameter of the confining container (Fig. 2, *Schemes*) (5, 8, 12, 17, 28, 29).

For a more quantitative study of the effect of droplet size on the spatial arrangement of encapsulated microtubules, we first categorized, by visual inspection, the arrangements observed 20 min after the start of nucleation (Fig. 2). In addition to "evenly distributed" microtubule arrays that fill the entire volume of the droplet (Fig. 2*A*) and "cortical arrangements" of microtubules, where most of the detected microtubule mass is close to the droplet boundary (Fig. 2*B*), we observed three other categories of microtubule arrays: an "opening cloud," which is similar to the cortical arrangement but with the main microtubule mass not as close to the droplet boundary and some microtubules also present in the droplet center (Fig. 2*C*); a "ring-like bundle" of microtubules that looks like a cortical arrangement confined to only two dimensions (Fig. 2*D*); and, finally, a "spoke-like arrangement" of microtubules characterized by straight microtubules having a high density in the droplet center, suggesting that microtubules with lengths in the range of the droplet diameter were present in random orientations (Fig. 2*E*).

Inspection of time courses revealed that the arrangements typically started from microtubules that were distributed evenly (Fig. 3 and supplemental Movies 3–7). Different pathways appeared to lead to different end configurations. In some droplets, the evenly distributed array stayed intact (Fig. 3*A* and supplemental Movie 3), and in others it transformed into a cortical arrangement (Fig. 3*B* and supplemental Movie 4) or into a single ring-like bundle (Fig. 3*C* and supplemental Movie 5). In other droplets, the evenly distributed array transformed into a spoke-like arrangement (Fig. 3*D* and supplemental Movie 6) that, in some cases, transformed again into an opening cloud of microtubules inside the lipid-monolayered droplets (Fig. 3*E* and supplemental Movie 7).

To better understand the potential mechanisms leading to these different transformations of the microtubule architectures in a confined geometry, we quantified the frequencies of these five categories as observed after 20 min in droplets of different size (Fig. 4*A*). A clear trend of how the final distributions of microtubule arrangements changed with droplet size was evident. The fraction of evenly distributed microtubule arrangements clearly increased with droplet size (Fig. 4*B*, *red*), suggesting that this arrangement prevails when microtubules are short in comparison to droplet diameter. In contrast, spoke-like arrangements and ring-like bundles were most frequent for the smallest droplets (Fig. 4*B*, *gray* and *black*, respectively), suggesting that these configurations potentially appear as a consequence of microtubules either failing to grow beyond the droplet diameter (spoke-like) or growing longer than the droplet diameter and then bending strongly (ring-like). The opening cloud and cortical arrangement were most frequent at intermediate droplet sizes within the examined range (Fig. 4*B*, *light blue* and *dark blue*, respectively), suggesting that these arrangements reflect a mild increase of microtubule length over droplet diameter (see "Discussion"). This overall trend of how arrangements changed with droplet size was insensitive to tubulin concentration, as shown by an analysis of the frequencies of the different microtubule arrangements for a reduced (Fig. 4*C*) and

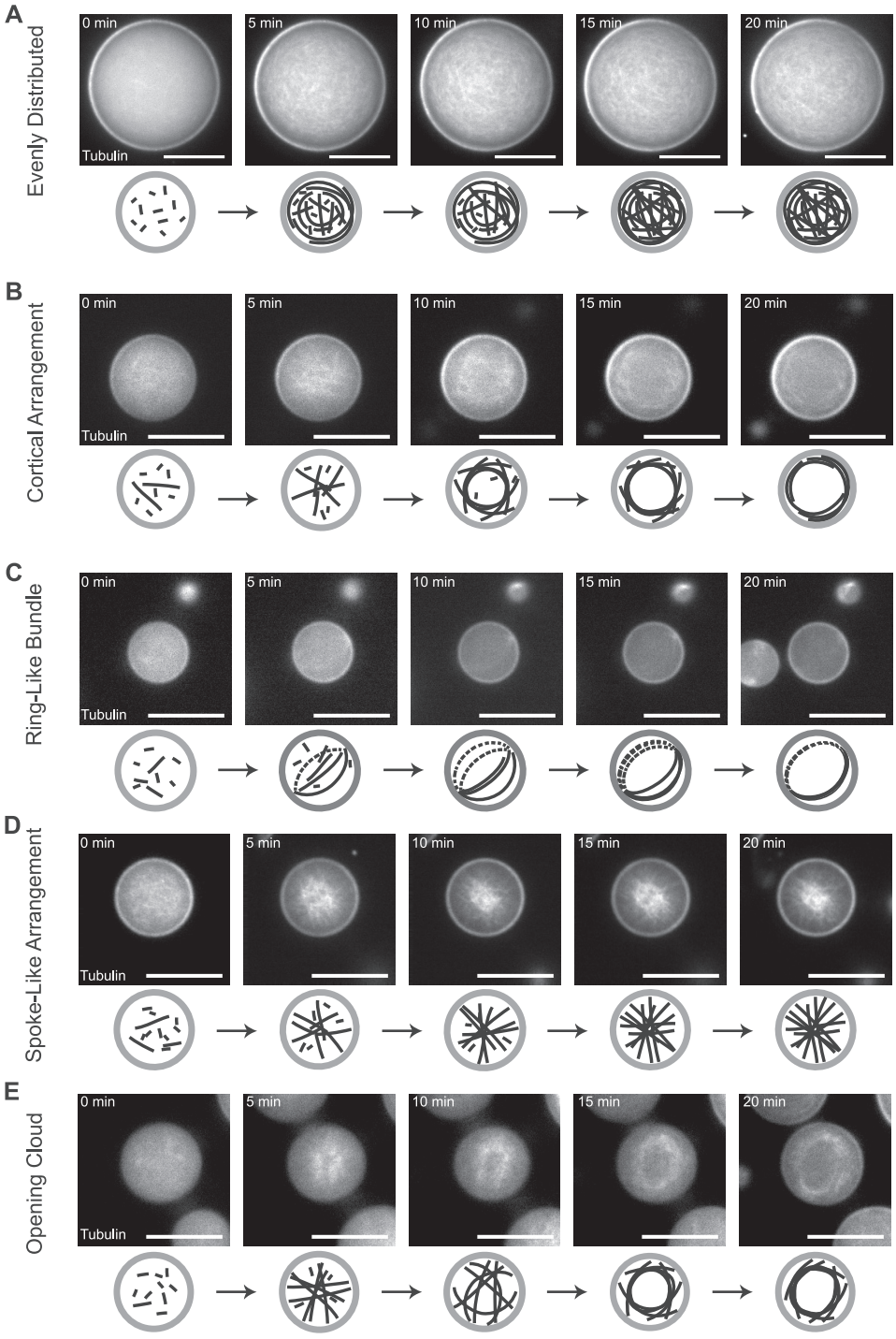

FIGURE 3. **Time course of confined microtubule arrangements: characteristic examples for the different arrangement categories.** *De novo* polymerization and formation of different arrangements of microtubules inside DOPC/DOPE/DOPG-monolayered droplets. Representative time series of spinning disk confocal microscopy images of confined microtubules polymerizing from 40 μM Atto633-tubulin in standard droplet buffer in response to a temperature shift to 32 °C. Examples for the different categories of arrangements are shown: network of evenly distributed microtubules (*A*), cortical arrangement (*B*), ring-like bundle (*C*), spoke-like arrangement (*D*), and opening cloud of microtubules (*E*). Schematics of the arrangements are shown *below* the experimental data. *Scale bars* = 20 μm.

an elevated (Fig. 4*D*) tubulin concentration. However, the distributions of arrangements were shifted systematically when the tubulin concentration was varied (Fig. 4, *C* and *D*), suggesting that changing the microtubule length-to-droplet diameter ratio causes the shifted distributions (see "Discussion").

Finally, we examined how the addition of a microtubule cross-linking motor affects microtubule organization in lipid-monolayered droplets. We used an mCherry-tagged minus end-directed kinesin-14, which has been used previously to study motor/microtubule self-organization in a quasi-unconfined situation (in a regular flow chamber) (4). This motor can organize microtubules into asters by sliding microtubules relative to each other and by eventually bringing minus ends together in focused poles (4, 6), somewhat similar to the role of

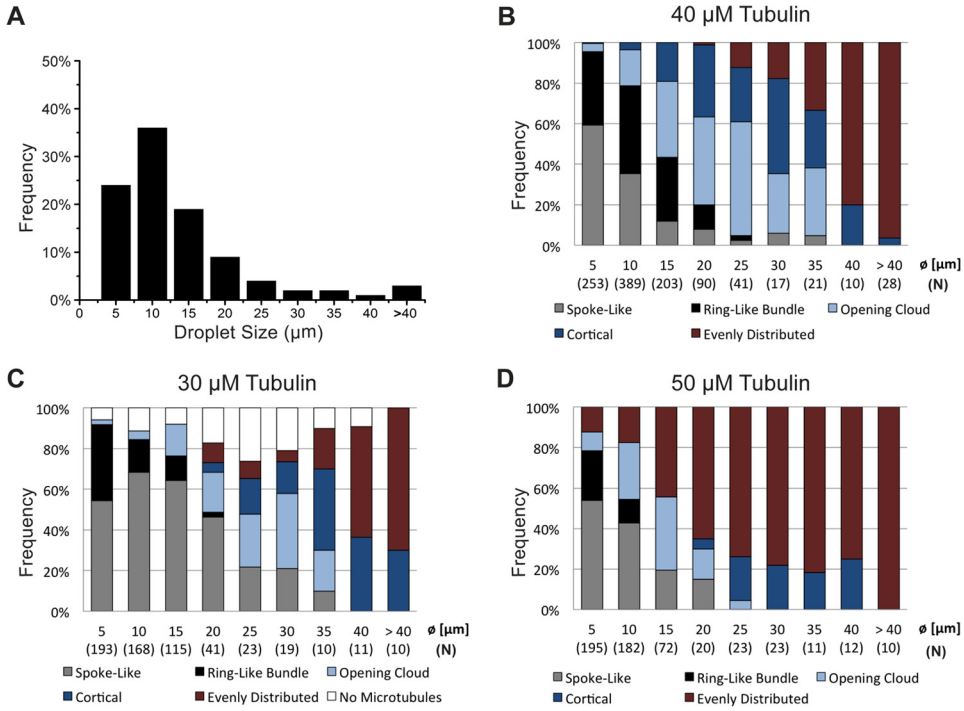

FIGURE 4. **Droplet size distribution and frequency of microtubule arrangements over droplet size.** *A*, histogram of the size distribution of observed DOPC/DOPE/DOPG-monolayered droplets. The bar graph displays the relative frequencies of the categories of formed microtubule arrangements after 20 min in droplets of different size, containing 40 (*B*), 30 (*C*), or 50 μM (*D*) tubulin in standard droplet buffer. Droplets were assigned to the diameter bins (*Ø*) as indicated. *Numbers in parentheses* indicate the total count (*N*) of droplets for each size category.

the motor in spindle pole formation in some cell types (7, 30–32). In a quasi-unconfined environment, kinesin-14-dependent microtubule organization leads to the formation of many asters (supplemental Movie 8). Under our conditions, typical final diameters of these motor-organized asters were in the range of 40 μm (supplemental Movie 8), similar to previous observations (4).

Encapsulation of mCherry-kinesin-14 together with Atto633-tubulin, GTP, and ATP in DOPC/DOPE/DOPG-monolayered droplets had a dramatic effect on the microtubule organizations we observed after 25 min, when the process of self-organization came to an end (Fig. 5 and supplemental Movies 9 and 10). In large droplets, single self-organized microtubule asters formed that filled the entire volume of the droplets (Figs. 5, *top panel*, and 6*A*, *top row*, and supplemental Movie 9). The motor localized weakly along microtubules and concentrated strongly in the center of the aster, as expected (4), indicating that the microtubule minus ends were focused into a pole. In smaller droplets ($<\sim$35 μm), "cortical bundles" formed, with the motors associating all along the strongly bundled microtubules (Fig. 6*A*, *center* and *bottom row*, and supplemental Movie 10). This indicates that the motor did not succeed in sorting the microtubules and, probably, that mostly randomly oriented bundles formed. In very small droplets ($<$15 μm), again, ring-like bundles were observed preferentially (Fig. 6*A*, *bottom row*). No spoke-like arrangements or opening cloud-like configurations were observed in the presence of the cross-linking motor, further highlighting its influence on the accessible microtubule configurations in this system.

Quantitative analysis of the relative frequencies of microtubule arrays in the presence of the motor confirmed a systematic change of the three organizations as a function of droplet size (Fig. 6*B*). Three sizes were found to be particularly selective for a certain type of microtubule organization: droplets with a diameter of around 5 μm, 25 μm, and above 40 μm had a very strong preference for ring-like bundles (Fig. 6*B*, *black*), cortical bundles (Fig. 6*B*, *blue*), and asters (Fig. 6*B*, *red*), respectively. The formation of single asters in larger droplets was robust (Fig. 7). Taken together, these results demonstrate the strong selective influence of confinement size on motor-mediated microtubule organization.

DISCUSSION

Here we have reconstituted for the first time from purified proteins motor-mediated microtubule aster self-organization in confined and lipid-monolayered volumes of micrometer dimensions. We investigated the conditions for optimal microtubule growth and the effect of the boundary on microtubule organization in the absence and presence of a microtubule cross-linking motor.

Lipid mixtures containing PC headgroups together with phosphatidylglycerol (PG) and/or phosphatidylethanolamine (PE) headgroups allowed microtubule growth, whereas DOPC alone mostly induced tubulin aggregation. This is potentially due to a previously reported interaction of tubulin with lipids having this headgroup (26, 33, 34), possibly causing tubulin unfolding and aggregation. Changed lipid headgroup interactions in the presence of PE or negatively charged lipids (35) or electrostatic repulsion by negatively charged lipids can probably alleviate that negative influence. Interactions of tubulin with lipids at the boundary could significantly deplete tubulin from solution, especially in smaller lipid-monolayered droplets (26,

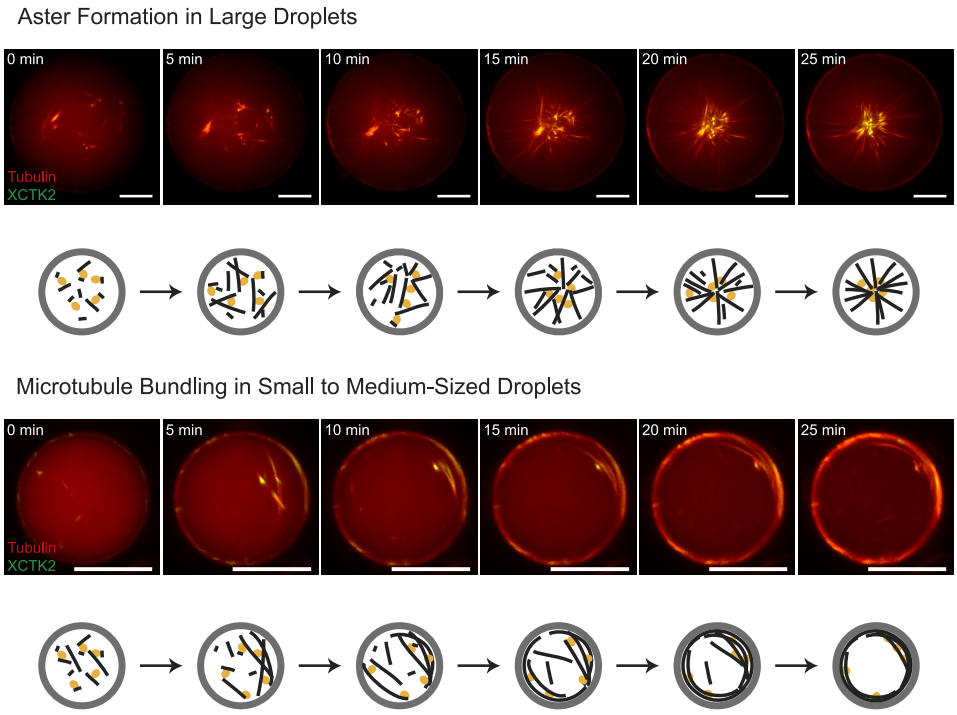

FIGURE 5. **Time course of confined motor-driven microtubule self-organization.** Shown is motor-driven microtubule self-organization inside DOPC/DOPE/DOPG-monolayered droplets of different sizes. Also shown is a time series of characteristic images of motor-driven microtubule organization inside a large (85-μm diameter, *top panel*) and a medium-sized (30-μm diameter, *bottom panel*) lipid-monolayered droplet containing 40 μM Atto633-labeled tubulin (*red*) and 200 nM mCherry-kinesin-14 (*green*) in standard droplet buffer, as acquired with spinning disk confocal microscopy at 32 °C. Schematics of the observed microtubule (*black*) and motor (*orange*) organizations inside droplets (*gray*) are shown *below* the experimental data. *Scale bars* = 20 μm.

33, 34, 36, 37). To overcome such boundary-induced effects and to ensure efficient nucleation and growth of microtubules in droplets, the tubulin concentration was increased in comparison with experiments outside of droplets, and the buffer was supplemented with glycerol as an additional nucleation promoting agent. The conditions used here allowed us to establish an experimental system in which microtubule organization in lipid-monolayered droplets could be studied reliably using confocal microscopy.

The probability of observing a certain microtubule arrangement depended on droplet size in a manner that can be rationalized by considering microtubule length and droplet diameter. The oil/water interface provides a rather rigid boundary for a microtubule (17). When growing microtubules touch the boundary with both of their ends, they will either stop growing or buckle if growth continues. The shorter the microtubule, the higher the buckling force will be (29, 38). This explains why the most frequent microtubule arrangement in the smallest droplets of this study (~5-μm diameter) was the spoke-like arrangement. This arrangement has not been reported in earlier experiments with microtubules growing in larger micrometer-sized confined geometries (10). Spoke-like arrangements apparently result from halting microtubule growth at the boundary because the polymerization force is smaller than the buckling force.

Another frequently observed configuration in small droplets was the ring-like bundle. Here the polymerization force was apparently large enough to allow microtubules to continue polymerizing, resulting in buckling. Most likely, this difference to similarly sized droplets with spoke-like arrangements is due to random differences in microtubule nucleation efficiency, a parameter that is typically not very well controlled in the absence of specific nucleating entities such as, for example, centrosomes or axonemes. Therefore, ring-like bundles might form in droplets where nucleation happens to be less efficient, resulting in higher remaining tubulin concentrations when (the fewer) microtubules reach the length of the droplet diameter, in turn leading to higher polymerization forces at this stage. Remarkably, the majority of these bent microtubules arrange into a single bundled ring, possibly because of steric reasons, reminiscent of mechanisms proposed to cause microtubule alignment in plant cells (39). Because highly bent microtubules in very small droplets are expected to be strongly pressed against the boundary, the microtubules might rather align instead of crossing each other (39, 40). Such an organization of confined filaments into rings has been observed previously for cross-linked actin filaments in liposomes (41).

With increasing droplet size in our experiments, spoke-like arrangements and ring-like bundles were observed less frequently, most likely because the microtubules could grow longer until they were confined by the boundary and, therefore, could buckle more easily and cross each other more easily at the boundary, possibly because they were not as strongly bent. This would explain why, in intermediate-sized droplets (~20- to 35-μm diameter), opening clouds and cortical arrangements of microtubules were observed most frequently; the difference between the two being largely the degree of microtubule bending. In comparison, for the reconstitution of cortical arrangements of the more flexible actin filaments in droplets, actin

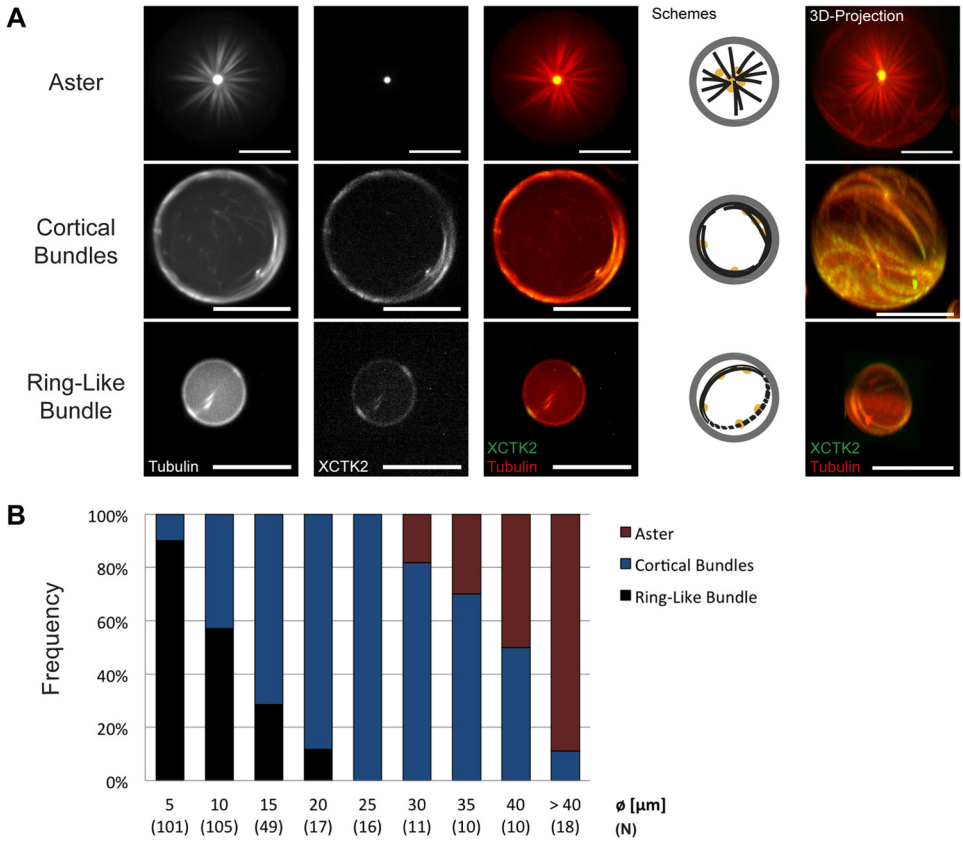

FIGURE 6. **Droplet size dependence of confined motor-driven microtubule self-organization.** *A*, different categories of end states. Spinning disk confocal microscopy images of DOPC/DOPE/DOPG-monolayered droplets containing 40 μM Atto633-labeled tubulin (*red* in merge) and 200 nM mCherry-kinesin-14 (*green* in merge) in standard droplet buffer taken 25 min after reaction start are shown. Single channel and merged channel images of the equatorial droplet plane are shown as indicated. The schematics display the arrangements of microtubules (*black*) and the localization of the motor protein (*orange*) inside lipid-monolayered droplets (*gray*). The images on the *right* show three-dimensional projections. *Scale bars* = 20 μm. *B*, bar graph displaying the relative frequencies of the motor-organized microtubule organizations for different droplet diameters (Ø). *Numbers in parentheses* indicate the total count (*N*) of droplets analyzed for each size category.

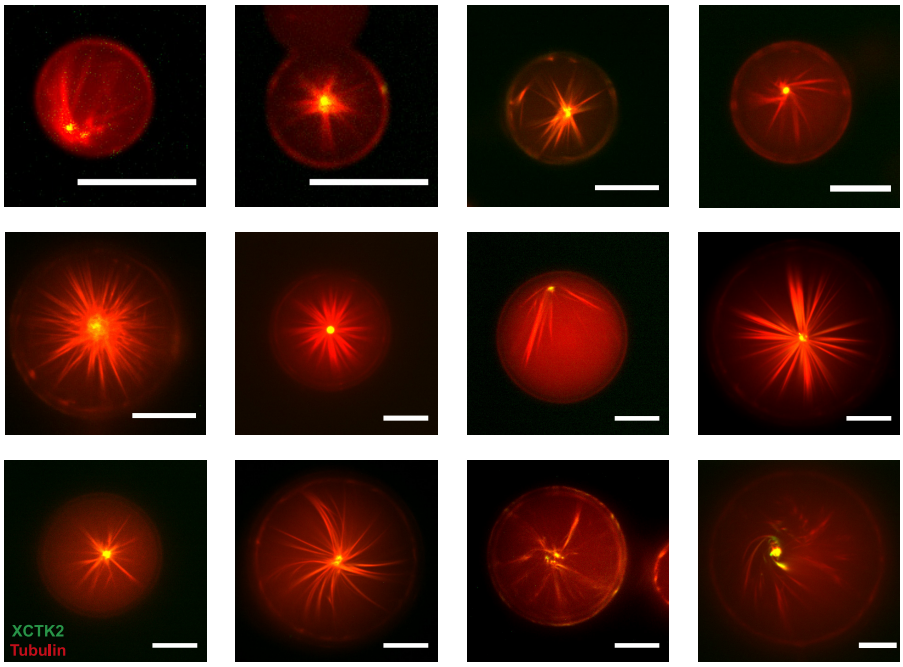

FIGURE 7. **Confined motor/microtubule self-organization into asters.** Merged spinning disk confocal microscopy images of large DOPC/DOPE/DOPG-monolayered droplets containing 40 μM Atto633-labelled tubulin (*red*) and 200 nM mCherry-XCTK2 (*green*) in standard droplet buffer taken 25 min after reaction start are shown. *Scale bars* = 20 μm.

binding proteins were linked directly to the droplet boundary (15, 16).

The above considerations can also rationalize the pathways along which the different arrangements formed. To produce cortical arrangements, initially, spoke-like arrangements progressed into opening clouds (beginning microtubule buckling) that then transformed to the final cortical arrangement (supplemental Movie 4). Opening clouds were also a prominent end state, probably in situations when microtubules were not able to buckle more. Overall, the influence of confinement in the medium-sized droplets observed here agrees well with previously established concepts developed in simulations and experiments in microfabricated chambers of the 25- to 35-μm diameter range (10). Finally, in very large droplets ($>\sim$40 μm), mostly even distributions of microtubules were observed. This observation indicates that in large droplets most microtubules stopped growing before they reached the length of the droplet diameter. This situation is similar to aster organization in bulk solution, suggesting that under our conditions at the droplet size of about $\sim$40 μm the organizing influence of the boundary becomes negligible.

In living cells, molecular motors play an important role for microtubule organization by cross-linking and sliding microtubules (7, 30–32). *In vitro* motile cross-linkers have been shown in quasi-two dimensional environments to organize microtubules into asters with a focused pole (4–6) or into vortices with bent microtubules positioned around a central hole, depending on how efficiently the motors can stay bound to microtubule ends (6). Early motor-microtubule self-organization experiments in microfabricated chambers reported that aster formation by an artificially oligomerized plus-end directed kinesin-1 construct occurred as an intermediate state, finally leading to vortex formation (5). Here, using kinesin-14, which has been shown previously to efficiently organize microtubules into asters *in vitro* in the absence of confinement (6), we showed that purified microtubules and motors can stably self-organize into astral arrays inside a confined micrometer-sized volume.

Our results demonstrate that, for droplets in the range of $\sim$40–100 μm, motor-mediated self-organization is an efficient method to generate exactly one aster in a confined volume (Fig. 7). Alternatively, single microtubule asters can also be produced in micrometer-sized volumes by coencapsulating purified centrosomes or artificial nucleating centers (11, 12). However, currently it is not easy to precisely control the number of centrosomes or nucleation centers in micrometer-sized confined volumes.

We observed that self-organized asters formed only when the droplets were large enough, the requirement apparently being that the droplet diameter must be at least twice the typical length of the microtubules. Occasionally, slightly distorted asters with bent microtubules were observed when the container size was apparently slightly too small (Fig. 7). In much smaller volumes, motors failed to organize microtubules into asters and only bundled the microtubules, emphasizing again the contribution of confinement toward organization. We have not observed pronounced vortex formations, most likely because the motor we used has a strong tendency to bring microtubule ends together, strongly favoring aster over vortex formation (4, 6).

Interestingly, the combined constraints of motor sliding and geometric confinement did not only allow a new self-organized state (the aster) in comparison with the situation without the motor, but, at the same time, also reduced the total number of accessible microtubule arrangements. Most likely, due to the bundling activity of the motor, opening clouds and cortical arrangements were replaced by cortical bundles, *i.e.* highly bundled, bent microtubules. Remarkably, no spoke-like arrangements were observed in the presence of the cross-linking motor (Fig. 6). This is probably due to motor-mediated microtubule bundling and sliding of antiparallel microtubules in the bundles contributing an additional force (in addition to the polymerization force) that can increase bundle length and lead to bundle buckling when bundles reach the length of the droplet diameter. This indicates that microtubule sliding also has an organizing influence in small droplets where asters cannot self-organize.

Our results obtained with a small set of purified components are in line with the previously observed microtubule arrangements in egg PC-monolayered droplets filled with *Xenopus* egg extract. In such an extract, the dynein complex, together with several other proteins (*e.g.* dynactin, Lis1, or NuMA), focuses microtubule minus ends into poles (18, 19, 42). In that system, radial asters formed predominantly in droplets larger than $\sim$30 μm, whereas distorted asters with one pole pushed toward the droplet boundary were observed at intermediate droplet sizes of $\sim$10–30 μm. Such mispositioned asters were less frequently observed in our experiments, probably because the microtubules were not dynamic because of the presence of stabilizing agents such as paclitaxel and glycerol (25, 43), which we added to promote efficient microtubule nucleation. In contrast, microtubules in *Xenopus* egg extract nucleate efficiently and are highly dynamic because of the presence of a multitude of microtubule nucleation and dynamics regulating proteins (3).

Similar to our experiments with purified components, in previous *Xenopus* egg extract droplets, only cortically arranged microtubule bundles were observed when the droplet diameter was less than $\sim$10 μm. The absence of spoke-like arrangements and opening clouds in *Xenopus* egg extract droplets is readily explained by the presence of the bundling and sliding activity of motors. Therefore, the predominant microtubule organizations, asters and cortical bundles, observed in an encapsulated egg extract with a complex protein composition can be recapitulated faithfully in a well defined *in vitro* system containing encapsulated tubulin and a cross-linking motor only.

These two types of microtubule organization forms are also prominent in living cells. Cortical arrangements are typical for many plant cells. Microtubule buckling as a consequence of spatial constraints as well as microtubule cross-linking by specific motors together with steric alignment have been proposed as organizational principles (8, 17, 28, 29, 39). In elongated plant cells, additional control mechanisms are needed to determine the preferred orientation of the microtubule bundles with respect to the long axis of the cell (10, 44–47).

Microtubule asters are typical for many differentiated metazoan interphase cells, *e.g.* human fibroblasts, and for dividing

metazoan cells around spindle poles. Naturally, either centrosomes and/or minus-end-directed motor proteins like kinesin-14 or dynein are needed for astral microtubule array formation in cells (30–32). Our *in vitro* system has incorporated the organizing activity of kinesin-14 as a strong morphogenetic factor, whereas control of nucleation was achieved by adding microtubule stabilizing agents. In the future, it will be interesting to add natural nucleators and microtubule dynamics regulators to mimic the natural situation more closely. In addition, local regulation of dynamic microtubule properties at the boundary (48) and motor-dependent sliding or positioning of the assembled array by pulling forces at the boundary (49) are some of the other important activities that were still absent in our minimal *in vitro* system.

In conclusion, using lipid-monolayered droplets in oil, we established an experimental system that allowed the study of the self-organization of motors and microtubules in three-dimensional volumes in the size range of tens of micrometers, similar to the size range of living eukaryotic cells. Droplet size determined whether minus end-directed, microtubule cross-linking motors organized microtubules into asters or into cortical bundles, two characteristically different microtubule organizations found in different living cells. Our system can be extended directly using the reverse emulsion method (14) to transform the current lipid-monolayered droplets in oil into liposomes with a deformable lipid bilayer membrane, mimicking more closely the boundary of a living cell.

Acknowledgments—We thank Léa-Laetitia Pontani and Cécile Sykes for help with setting up the droplet-in-oil assay; Christian Hentrich and Surajit Ghosh for protein purification advice and assay development; Iris Lueke for cell culture and protein purification; Nicholas Cade for microscopy support; and Peter Bieling, Christoph Feest, Natalia Goehring, Banafshe Larijani, and Michael Vahey for discussions and advice.

REFERENCES

1. Deinum, E. E., and Mulder, B. M. (2013) Modelling the role of microtubules in plant cell morphology. *Curr. Opin. Plant Biol.* **16,** 688–692
2. Dogterom, M., and Surrey, T. (2013) Microtubule organization *in vitro*. *Curr. Opin. Cell Biol.* **25,** 23–29
3. Helmke, K. J., Heald, R., and Wilbur, J. D. (2013) Interplay between spindle architecture and function. *Int. Rev. Cell Mol. Biol.* **306,** 83–125
4. Hentrich, C., and Surrey, T. (2010) Microtubule organization by the antagonistic mitotic motors kinesin-5 and kinesin-14. *J. Cell Biol.* **189,** 465–480
5. Nédélec, F. J., Surrey, T., Maggs, A. C., and Leibler, S. (1997) Self-organization of microtubules and motors. *Nature* **389,** 305–308
6. Surrey, T., Nedelec, F., Leibler, S., and Karsenti, E. (2001) Physical properties determining self-organization of motors and microtubules. *Science* **292,** 1167–1171
7. Fink, G., Hajdo, L., Skowronek, K. J., Reuther, C., Kasprzak, A. A., and Diez, S. (2009) The mitotic kinesin-14 Ncd drives directional microtubule-microtubule sliding. *Nat. Cell Biol.* **11,** 717–723
8. Elbaum, M., Kuchnir Fygenson, D., and Libchaber, A. (1996) Buckling microtubules in vesicles. *Phys. Rev. Lett.* **76,** 4078–4081
9. Fygenson, D. K., Marko, J. F., and Libchaber, A. (1997) Mechanics of microtubule-based membrane extension. *Phys. Rev. Lett.* **79,** 4497–4500
10. Cosentino Lagomarsino, M., Tanase, C., Vos, J. W., Emons, A. M., Mulder, B. M., and Dogterom, M. (2007) Microtubule organization in three-dimensional confined geometries: evaluating the role of elasticity through a combined *in vitro* and modeling approach. *Biophys. J.* **92,** 1046–1057
11. Faivre-Moskalenko, C., and Dogterom, M. (2002) Dynamics of microtubule asters in microfabricated chambers: the role of catastrophes. *Proc. Natl. Acad. Sci. U.S.A.* **99,** 16788–16793
12. Holy, T. E., Dogterom, M., Yurke, B., and Leibler, S. (1997) Assembly and positioning of microtubule asters in microfabricated chambers. *Proc. Natl. Acad. Sci. U.S.A.* **94,** 6228–6231
13. Griffiths, A. D., and Tawfik, D. S. (2006) Miniaturising the laboratory in emulsion droplets. *Trends Biotechnol.* **24,** 395–402
14. Pautot, S., Frisken, B. J., and Weitz, D. A. (2003) Production of unilamellar vesicles using an inverted emulsion. *Langmuir* **19,** 2870–2879
15. Pontani, L. L., van der Gucht, J., Salbreux, G., Heuvingh, J., Joanny, J. F., and Sykes, C. (2009) Reconstitution of an actin cortex inside a liposome. *Biophys. J.* **96,** 192–198
16. Abu Shah, E., and Keren, K. (2014) Symmetry breaking in reconstituted actin cortices. *eLife* **3,** e01433
17. Pinot, M., Chesnel, F., Kubiak, J. Z., Arnal, I., Nedelec, F. J., and Gueroui, Z. (2009) Effects of confinement on the self-organization of microtubules and motors. *Curr. Biol.* **19,** 954–960
18. Merdes, A., Ramyar, K., Vechio, J. D., and Cleveland, D. W. (1996) A complex of NuMA and cytoplasmic dynein is essential for mitotic spindle assembly. *Cell* **87,** 447–458
19. Heald, R., Tournebize, R., Blank, T., Sandaltzopoulos, R., Becker, P., Hyman, A., and Karsenti, E. (1996) Self-organization of microtubules into bipolar spindles around artificial chromosomes in *Xenopus* egg extracts. *Nature* **382,** 420–425
20. Hyman, A., Drechsel, D., Kellogg, D., Salser, S., Sawin, K., Steffen, P., Wordeman, L., and Mitchison, T. (1991) Preparation of modified tubulins. *Methods Enzymol.* **196,** 478–485
21. Castoldi, M., and Popov, A. V. (2003) Purification of brain tubulin through two cycles of polymerization-depolymerization in a high-molarity buffer. *Protein Expr. Purif.* **32,** 83–88
22. Ghosh, S., Hentrich, C., and Surrey, T. (2013) Micropattern-controlled local microtubule nucleation, transport, and mesoscale organization. *ACS Chem. Biol.* **8,** 673–678
23. Bieling, P., Telley, I. A., Hentrich, C., Piehler, J., and Surrey, T. (2010) Fluorescence microscopy assays on chemically functionalized surfaces for quantitative imaging of microtubule, motor, and +TIP dynamics. *Methods Cell Biol.* **95,** 555–580
24. van Meer, G., Voelker, D. R., and Feigenson, G. W. (2008) Membrane lipids: where they are and how they behave. *Nat. Rev. Mol. Cell Biol.* **9,** 112–124
25. Shelanski, M. L., Gaskin, F., and Cantor, C. R. (1973) Microtubule assembly in the absence of added nucleotides. *Proc. Natl. Acad. Sci. U.S.A.* **70,** 765–768
26. Wolff, J. (2009) Plasma membrane tubulin. *Biochim. Biophys. Acta* **1788,** 1415–1433
27. Larijani, B., Poccia, D. L., and Dickinson, L. C. (2000) Phospholipid identification and quantification of membrane vesicle subfractions by 31P-1H two-dimensional nuclear magnetic resonance. *Lipids* **35,** 1289–1297
28. Dogterom, M., Kerssemakers, J. W., Romet-Lemonne, G., and Janson, M. E. (2005) Force generation by dynamic microtubules. *Curr. Opin. Cell Biol.* **17,** 67–74
29. Gittes, F., Mickey, B., Nettleton, J., and Howard, J. (1993) Flexural rigidity of microtubules and actin filaments measured from thermal fluctuations in shape. *J. Cell Biol.* **120,** 923–934
30. Cai, S., Weaver, L. N., Ems-McClung, S. C., and Walczak, C. E. (2009) Kinesin-14 family proteins HSET/XCTK2 control spindle length by cross-linking and sliding microtubules. *Mol. Biol. Cell* **20,** 1348–1359
31. Vorobjev, I., Malikov, V., and Rodionov, V. (2001) Self-organization of a radial microtubule array by dynein-dependent nucleation of microtubules. *Proc. Natl. Acad. Sci. U.S.A.* **98,** 10160–10165
32. Walczak, C. E., Verma, S., and Mitchison, T. J. (1997) XCTK2: a kinesin-related protein that promotes mitotic spindle assembly in *Xenopus laevis* egg extracts. *J. Cell Biol.* **136,** 859–870
33. Klausner, R. D., Kumar, N., Weinstein, J. N., Blumenthal, R., and Flavin, M. (1981) Interaction of tubulin with phospholipid vesicles: I: association with vesicles at the phase transition. *J. Biol. Chem.* **256,** 5879–5885

34. Kumar, N., Klausner, R. D., Weinstein, J. N., Blumenthal, R., and Flavin, M. (1981) Interaction of tubulin with phospholipid vesicles: II: physical changes of the protein. *J. Biol. Chem.* **256,** 5886–5889
35. McIntosh, T. J., and Simon, S. A. (1994) Hydration and steric pressures between phospholipid bilayers. *Annu. Rev. Biophys. Biomol. Struct.* **23,** 27–51
36. Caron, J. M., and Berlin, R. D. (1987) Dynamic interactions between microtubules and artificial membranes. *Biochemistry* **26,** 3681–3688
37. Rostovtseva, T. K., Gurnev, P. A., Chen, M. Y., and Bezrukov, S. M. (2012) Membrane lipid composition regulates tubulin interaction with mitochondrial voltage-dependent anion channel. *J. Biol. Chem.* **287,** 29589–29598
38. Dogterom, M., and Yurke, B. (1997) Measurement of the force-velocity relation for growing microtubules. *Science* **278,** 856–860
39. Hawkins, R. J., Tindemans, S. H., and Mulder, B. M. (2010) Model for the orientational ordering of the plant microtubule cortical array. *Phys. Rev. E Stat. Nonlin. Soft Matter Phys.* **82,** 011911
40. Allard, J. F., Wasteneys, G. O., and Cytrynbaum, E. N. (2010) Mechanisms of self-organization of cortical microtubules in plants revealed by computational simulations. *Mol. Biol. Cell* **21,** 278–286
41. Limozin, L., and Sackmann, E. (2002) Polymorphism of cross-linked actin networks in giant vesicles. *Phys. Rev. Lett.* **89,** 168103
42. Wang, S., Ketcham, S. A., Schön, A., Goodman, B., Wang, Y., Yates, J., 3rd, Freire, E., Schroer, T. A., and Zheng, Y. (2013) Nudel/NudE and Lis1 promote dynein and dynactin interaction in the context of spindle morphogenesis. *Mol. Biol. Cell* **24,** 3522–3533
43. Schiff, P. B., Fant, J., and Horwitz, S. B. (1979) Promotion of microtubule assembly *in vitro* by taxol. *Nature* **277,** 665–667
44. Ambrose, C., Allard, J. F., Cytrynbaum, E. N., and Wasteneys, G. O. (2011) A CLASP-modulated cell edge barrier mechanism drives cell-wide cortical microtubule organization in *Arabidopsis*. *Nat. Commun.* **2,** 430
45. Wasteneys, G. O., and Ambrose, J. C. (2009) Spatial organization of plant cortical microtubules: close encounters of the 2D kind. *Trends Cell Biol.* **19,** 62–71
46. Lindeboom, J. J., Lioutas, A., Deinum, E. E., Tindemans, S. H., Ehrhardt, D. W., Emons, A. M., Vos, J. W., and Mulder, B. M. (2013) Cortical microtubule arrays are initiated from a nonrandom prepattern driven by atypical microtubule initiation. *Plant Physiol.* **161,** 1189–1201
47. Nakamura, M., Ehrhardt, D. W., and Hashimoto, T. (2010) Microtubule and katanin-dependent dynamics of microtubule nucleation complexes in the acentrosomal *Arabidopsis* cortical array. *Nat. Cell Biol.* **12,** 1064–1070
48. Zhang, D., Grode, K. D., Stewman, S. F., Diaz-Valencia, J. D., Liebling, E., Rath, U., Riera, T., Currie, J. D., Buster, D. W., Asenjo, A. B., Sosa, H. J., Ross, J. L., Ma, A., Rogers, S. L., and Sharp, D. J. (2011) *Drosophila* katanin is a microtubule depolymerase that regulates cortical-microtubule plus-end interactions and cell migration. *Nat. Cell Biol.* **13,** 361–370
49. Laan, L., Pavin, N., Husson, J., Romet-Lemonne, G., van Duijn, M., López, M. P., Vale, R. D., Jülicher, F., Reck-Peterson, S. L., and Dogterom, M. (2012) Cortical dynein controls microtubule dynamics to generate pulling forces that position microtubule asters. *Cell* **148,** 502–514